AGU PUBLICATIONS

Radio Science

RESEARCH ARTICLE
10.1002/2016RS006158

Key Points:
- We derive the log-likelihood function of the received signal for the target in a Rice fading environment
- The joint MCRLB of target position and velocity for OFDM-based passive radar networks in a Rice fading environment is computed
- We reveal the relationships between the joint MCRLB and various factors

Correspondence to:
J. J. Zhou,
zjjee@nuaa.edu.cn

Citation:
Shi, C. G., S. Salous, F. Wang, and J. J. Zhou (2017), Modified Cramér-Rao lower bounds for joint position and velocity estimation of a Rician target in OFDM-based passive radar networks, *Radio Sci.*, *52*, 15–33, doi:10.1002/2016RS006158.

Received 25 AUG 2016
Accepted 17 NOV 2016
Accepted article online 7 DEC 2016
Published online 7 JAN 2017

Modified Cramér-Rao lower bounds for joint position and velocity estimation of a Rician target in OFDM-based passive radar networks

C. G. Shi[1,2], S. Salous[2], F. Wang[1], and J. J. Zhou[1]

[1] Key Laboratory of Radar Imaging and Microwave Photonics, Ministry of Education, Nanjing University of Aeronautics and Astronautics, Nanjing, China, [2] School of Engineering and Computing Sciences, Durham University, Durham, UK

Abstract Owing to the increased deployment and the favorable range and Doppler resolutions, orthogonal frequency-division multiplexing (OFDM)-based L band digital aeronautical communication system type 1 (LDACS1) stations have become attractive systems for target surveillance in passive radar applications. This paper investigates the problem of joint parameter (position and velocity) estimation of a Rician target in OFDM-based passive radar network systems with multichannel receivers placed on moving platforms, which are composed of multiple OFDM-based LDACS1 transmitters of opportunity and multiple radar receivers. The modified Cramér-Rao lower bounds (MCRLBs) on the Cartesian coordinates of target position and velocity are computed, where the received signal from the target is composed of dominant scatterer (DS) component and weak isotropic scatterers (WIS) component. Simulation results are provided to demonstrate that the target parameter estimation accuracy can be improved by exploiting the DS component. It also shows that the joint MCRLB is not only a function of the transmitted waveform parameters, target radar cross section, and signal-to-noise ratio but also a function of the relative geometry between the target and the passive radar networks. The analytical expressions of MCRLB can be utilized as a performance metric to access the target parameter estimation in OFDM-based passive radar networks in that they enable the selection of optimal transmitter-receiver pairs for target estimation.

1. Introduction

1.1. Background and Motivation

Distributed radar network systems, also known as spatial distributed multiple-input multiple-output (MIMO) radar systems [*Haimovich et al.*, 2008; *Li and Stoica*, 2009; *Pace*, 2009], attract contentiously growing attention nowadays and are on a path from theory to practical use due to signal and spatial diversities. Moreover, considerable research has been conducted into the potential use of radar networks for achieving performance improvement in various contexts such as target detection [*Fisher et al.*, 2006; *Naghsh et al.*, 2013], target localization [*Niu et al.*, 2012], target tracking [*Godrich et al.*, 2012b], waveform design [*Chen et al.*, 2013], sensor selection [*Godrich et al.*, 2012a], and information extraction [*Song et al.*, 2012].

Recently, extensive research [*Chen et al.*, 2015; *Daout et al.*, 2012; *Gogineni et al.*, 2014a; *Griffiths and Long*, 2014a; *Howland et al.*, 2005; *Stinco et al.*, 2012] has been conducted in passive radar systems that utilize illuminators of opportunity owing to their advantages of low implementation costs, low probability of intercept [*Shi et al.*, 2015, 2016c; *Zhang et al.*, 2015], and so on. The two-dimensional target localization problem is investigated for the WiFi-based multistatic passive radar [*Falcone et al.*, 2014], and different target localization schemes are proposed based on different sets of available measurements. *Alam and Jamil* [2015] propose a novel localization algorithm based on maximum likelihood (ML) for multistatic passive radar systems employing range-only measurements, which are solved by both gradient and Newton's decent methods. The work in [*Yi et al.*, 2015] presents a target tracking strategy to solve the measurement-to-transmitter association problem for a single frequency network-based MIMO passive radar, which can achieve low complexity and nearly optimal performance. *Gogineni et al.* [2014b] calculate the ambiguity functions for multistatic passive radar systems utilizing universal mobile telecommunications systems (UMTS) signals, in which both noncoherent and coherent processing modes are considered in the Cartesian domain. In *Samczynski et al.* [2015], the concept of passive radar using noncooperative pulse radars is proposed, and the experiment results are also provided. Furthermore, the authors in *Shi et al.* [2016b] propose two transmitter of opportunity subset

selection strategies for frequency modulation (FM)-based distributed passive radar network systems, which are formulated as knapsack problems and tackled with greedy selection approaches. Overall speaking, the previous studies have laid a solid foundation for the research of passive radar systems, and it should be mentioned that multiple signals of opportunity can be exploited as illuminators to remarkably improve the system performance.

The Cramér-Rao lower bound (CRLB) is an important performance metric for analyzing the local parameter estimation accuracy, which provides the smallest variance estimates of any unbiased estimators. It is introduced in *Godrich et al.* [2010] that the mean square error (MSE) of the maximum likelihood estimator (MLE) is close to the CRLB when certain conditions are satisfied. Recently, significant attention has been drawn to the CRLB for target parameter estimation with both noncoherent and coherent observations [*Godrich et al.*, 2010; *He and Blum*, 2010a; *He et al.*, 2010b, 2016; *Wei et al.*, 2010; *Zhao and Huang*, 2016]. In [*Godrich et al.*, 2010], the closed-form expressions of CRLB are derived for noncoherent and coherent MIMO radar systems, and it is demonstrated that the CRLB is inversely proportional to the carrier frequency and signals averaged effective bandwidth. *He et al.* [2010b] investigate the target parameter estimation performance for MIMO radar, and the joint position and velocity CRLB is derived. Later, they present the coherent processing case for joint target position and velocity estimation in MIMO radar [*He and Blum*, 2012], where it is shown that the coherent processing mode outperforms the noncoherent processing mode significantly. In *Wei et al.* [2010], the results in *He et al.* [2010b] are extended and the CRLB for multitarget noncoherent MIMO radar systems is computed. The work in *He and Blum* [2010a] studies the target localization accuracy for MIMO radar systems with static phase errors. *Zhao and Huang* [2016] compute the CRLBs for the joint time delay and Doppler stretch estimation of an extended target, which analyzes the effects of waveform parameters on the CRLB of both the time delay and the Doppler stretch for the extended target. In *Gogineni et al.* [2014b], *Stinco et al.* [2012], *Filip and Shutin*, 2016, *He and Blum*, 2014, 2016, *Javed et al.* [2016], and *Shi et al.* [2016a], the CRLB has been investigated and applied to passive radar systems employing Gaussian pulse signals, FM commercial radio signals, UMTS signals, global system for mobile communications (GSM) signals, and orthogonal frequency-division multiplexing (OFDM)-based L band digital aeronautical communication system type 1 (LDACS1) communication signals as signals of opportunity for the passive radar networks implementation. In *He et al.* [2016], a generalized CRLB and mismatched CRLB for distributed active and passive radar networks are derived, where it is assumed that the approximation state of the target is unknown without previous target detection. *Shi et al.* [2016a] presents the CRLB analysis for the joint target estimation of position and velocity in FM-based passive radar networks. In *Filip and Shutin* [2016], *Gogineni et al.* [2014a], and *Stinco et al.* [2012], the modified CRLB (MCRLB) is used as a good alternative to the classical CRLB due to the presence of random parameters in the transmitted waveforms, which has been shown to provide a looser bound in practical applications. The authors in *Javed et al.* [2016] address the target estimation performance of a UMTS-based passive multistatic radar system in a Rice fading environment, where the received signal from the target is composed of a dominant scatterer (DS) component and weak isotropic scatterers (WIS) component.

1.2. Major Contributions

On the basis of the previous works, almost all the studies focus on stationary platforms. In this study, we use the OFDM-based LDACS1 communication signals as signals of opportunity, which are exemplary OFDM signals with favorable range and Doppler resolutions. In addition, the Rician target model can cover a broad range of Swerling 0-V target radar cross section (RCS) models [*Patzold and Rafiq*, 2014]. To the best of the authors' knowledge, the CRLB for the joint position and velocity estimation of a Rician target in OFDM-based passive radar networks with multichannel radar receivers placed on moving platforms, which has not been considered, needs to be investigated. The OFDM-based passive radar networks are composed of multiple OFDM-based LDACS1 transmitters of opportunity and multiple radar receivers, and it is assumed that the scattered echoes from the target due to different OFDM-based illuminators of opportunity can be received and separated at the multichannel receivers. Since the transmitted data symbols are nondeterministic, we will compute the MCRLB for the joint Rician target estimation in a passive radar network, which can provide a quantitative measure of the networks performance.

To be specific, the contributions of this paper are as follows:

1. The joint MCRLB on the Cartesian coordinates of target position and velocity for OFDM-based passive radar networks in a Rice fading environment is computed, which is composed of multiple OFDM-based LDACS1 transmitters of opportunity and multiple radar receivers with antennas placed on moving platforms.

The main work of this paper are the derivations of the parameters needed to calculate the OFDM-based MCRLB in a Rice fading environment, which are a much more generalized case than that in *Filip and Shutin* [2016] and quite different from the results in *Javed et al.* [2016]. It is worth mentioning that the obtained results are valid for any general OFDM signals.

2. The analytical expressions of MCRLB can be utilized as a unified performance metric to access the target parameter estimation in any passive radar network systems employing OFDM-based signals of opportunity. Since the DS component may exist only for a subset of transmitter-receiver pairs, the choice of a transmitter-receiver pair has remarkable effect on the target estimation accuracy. Therefore, the geometry-dependent MCRLB will open up a new dimension for OFDM-based passive radar network systems by aiding the selection of optimal transmitter-receiver pairs to achieve a required estimation performance.
3. We also reveal the relationships between the joint MCRLB and various factors. It is shown that the joint MCRLB is a function of the transmitted waveform parameters as well as the relative geometry between the target and the passive radar networks. Moreover, it is also dependent on the target's RCS and SNR.

1.3. Outline of the Paper

The remainder of this paper is organized as follows. In section 2, the signal and system model for OFDM-based passive radar networks is introduced. Furthermore, the closed-form expressions of the joint MCRLBs for the Rician target position and velocity are computed in section 3. Numerical simulations are provided to demonstrate our analytical results in section 4. Finally, section 5 concludes this paper with potential future work.

Notation: The superscript † represents the transpose operator; $\mathbb{E}\{\cdot\}$ and $(\cdot)^*$ represent the expectation and conjugation operators, respectively. $|\cdot|$ denotes the absolute value, and $\Re\{\cdot\}$ is the real part. $U_i(f)$ denotes the Fourier transform of $u_i(t)$.

2. Signal Model

Let us consider a passive radar network architecture in a two-dimensional Cartesian space consisting of N_t transmitters and N_r multichannel receivers. We suppose that the ith transmitter and the jth receiver are located at $\overrightarrow{\mathbf{p}}_i^t = [x_i^t, y_i^t]$ and $\overrightarrow{\mathbf{p}}_j^r = [x_j^r, y_j^r]$, respectively. The target position and velocity are supposed to be deterministic unknown and denoted by $\overrightarrow{\mathbf{p}} = [x, y]$ and $\overrightarrow{\mathbf{v}} = [v_x, v_y]$. We define the target state vector to collect the target position and velocity as follows:

$$\boldsymbol{\Theta} = [x, y, v_x, v_y]^\dagger. \tag{1}$$

Without loss of generality, we will focus on a single target scenario. However, the results can be extended to multiple targets. The baseband signal transmitted by the ith transmitter can be expressed as [*Filip and Shutin*, 2016]:

$$u_i(t) = \sum_{l=0}^{L-1} \sum_{k=-N_u/2}^{N_u/2-1} c_{kl} e^{j2\pi k\Delta f(t-T_{cp}-lT_s)} w(t-lT_s) e^{j2\pi iBt}, \tag{2}$$

where c_{kl} denotes the transmitted data symbols, L is the total number of the transmitted OFDM symbols, N_u is the number of subcarriers, Δf is the subcarrier spacing, T_s is the total symbol duration, T_{cp} is the cyclic prefix in OFDM signal, and B is the signal bandwidth. $w(t)$ stands for the standard raised-cosine window given as

$$w(t) = \begin{cases} \frac{1}{2}\left(1+\cos\left(\frac{\pi}{T_w}(t-T_w)\right)\right), & 0 \le t < T_w, \\ 1, & T_w \le t < T_s, \\ \frac{1}{2}\left(1+\cos\left(\frac{\pi}{T_w}(t-T_s)\right)\right), & T_s \le t < T_{tot}, \\ 0, & \text{elsewhere}, \end{cases} \tag{3}$$

where T_w is the windowing duration and T_{tot} is the total length of one OFDM symbol. For uncorrelated data symbols over both the subcarrier and symbol indices we have

$$\mathbb{E}\left\{c_{kl}c_{mn}^*\right\} = \begin{cases} \frac{1}{LN_u(T_s-T_w/4)}, & k=m, l=n, \\ 0, & \text{elsewhere}. \end{cases} \tag{4}$$

It is assumed that the signals from different transmitters can be perfectly estimated at each receiver from the direct path reception and separated in some domain (for example, different frequency spectra) [*Gogineni et al.*, 2014a].

Let τ_{ij} represent the bistatic time delays corresponding to the path between the ith OFDM-based transmitter of opportunity, moving target, and the jth radar receiver with the target located at $\vec{\mathbf{p}} = [x, y]$:

$$\begin{aligned}\tau_{ij} &= \frac{\sqrt{\left(x_i^t - x\right)^2 + \left(y_i^t - y\right)^2} + \sqrt{\left(x_j^r - x\right)^2 + \left(y_j^r - y\right)^2}}{c} \\ &= \frac{\left\|\vec{\mathbf{p}} - \vec{\mathbf{p}}_i^t\right\| + \left\|\vec{\mathbf{p}} - \vec{\mathbf{p}}_j^r\right\|}{c},\end{aligned} \tag{5}$$

where c is the speed of light, $\left\|\vec{\mathbf{p}} - \vec{\mathbf{p}}_i^t\right\|$ is the distance from the ith transmitter to the target, and $\left\|\vec{\mathbf{p}} - \vec{\mathbf{p}}_j^r\right\|$ is the distance from the target to the jth receiver, respectively. In this paper, the multichannel radar receiver j moves with velocity $\vec{\mathbf{v}}_j^r = [v_{x,j}^r, v_{y,j}^r]$. With the mentioned positions/velocities of the target and radar receivers above, the Doppler shift of the moving target corresponding to the ijth path can be calculated as follows:

$$f_{D_{ij}} = \frac{f_c}{c}\left[\frac{\partial\left\|\vec{\mathbf{p}} - \vec{\mathbf{p}}_i^t\right\|}{\partial t} + \frac{\partial\left\|\vec{\mathbf{p}} - \vec{\mathbf{p}}_j^r\right\|}{\partial t}\right], \tag{6}$$

where f_c represents the carrier frequency. The terms $\frac{\partial\|\vec{\mathbf{p}} - \vec{\mathbf{p}}_i^t\|}{\partial t}$ and $\frac{\partial\|\vec{\mathbf{p}} - \vec{\mathbf{p}}_j^r\|}{\partial t}$ stand for the relative velocities for the ith transmitter of opportunity and the jth radar receiver, respectively. Thus, we can obtain

$$\begin{aligned}f_{D_{ij}} = &\frac{f_c}{c}\left[v_x\left(\frac{x - x_i^t}{\left\|\vec{\mathbf{p}} - \vec{\mathbf{p}}_i^t\right\|} + \frac{x - x_j^r}{\left\|\vec{\mathbf{p}} - \vec{\mathbf{p}}_j^r\right\|}\right)\right] + \frac{f_c}{c}\left[v_y\left(\frac{y - y_i^t}{\left\|\vec{\mathbf{p}} - \vec{\mathbf{p}}_i^t\right\|} + \frac{y - y_j^r}{\left\|\vec{\mathbf{p}} - \vec{\mathbf{p}}_j^r\right\|}\right)\right] \\ &+ \frac{f_c}{c}\left[v_{x,j}^r\frac{x - x_j^r}{\left\|\vec{\mathbf{p}} - \vec{\mathbf{p}}_j^r\right\|} + v_{y,j}^r\frac{y - y_j^r}{\left\|\vec{\mathbf{p}} - \vec{\mathbf{p}}_j^r\right\|}\right].\end{aligned} \tag{7}$$

It is worth mentioning that these transformation relations between the delay-Doppler space and the Cartesian coordinates are necessary while computing the MCRLB [*Gogineni et al.*, 2014a].

3. Joint MCRLB

In this section, the MCRLB for the joint target parameter estimation in OFDM-based passive radar networks is computed by deriving the modified Fisher information matrix (MFIM) expression, where it is assumed that the echoes scattered off the target due to different transmitters of opportunity can be separated at the multichannel radar receivers. Here using the Rician target model [*Javed et al.*, 2016], the attenuation coefficients ξ_{ij} can be modeled as a complex Gaussian random variable with mean a_{ij} and variance σ^2, i.e., $\xi_{ij} \sim \mathcal{CN}(a_{ij}, \sigma^2)$, which is composed of a DS and many independent WIS. The signal arriving at the jth receiver due to the signal transmitted from the ith OFDM-based transmitter of opportunity is written as

$$y_{ij}(t) = \xi_{ij}u_i(t - \tau_{ij})e^{j2\pi f_{D_{ij}}(t-\tau_{ij})} + n_{ij}(t), \tag{8}$$

where $n_{ij}(t)$ represents zero-mean white Gaussian noise of variance σ_n^2 corresponding to the ijth path, i.e., $n_{ij} \sim \mathcal{CN}(0, \sigma_n^2)$, independent to ξ_{ij}. The parameters a_{ij}, σ^2 and σ_n^2 are supposed to be deterministic and known.

It should be pointed out that the transmitted symbol $\mathbf{c}$ is not deterministic. Following the derivations in *Filip and Shutin* [2016], *Javed et al.* [2016], and *Van Trees* [2001], the MLE of the unknown target state vector $\boldsymbol{\Theta}$ can be found by examining the likelihood ratio for the hypothesis pair, with H_1 corresponding to the target presence hypothesis and H_0 corresponding to the noise only hypothesis. Thus, for a given transmitted symbol $\mathbf{c}$, the likelihood ratio corresponding to the ijth transmitter-receiver pair is

$$\begin{aligned}\Lambda_{ij}(y_{ij}(t)|\mathbf{c}) = \exp\Bigg\{&\frac{\sigma^2}{\sigma^2 + \sigma_n^2}\left|\int_{-\infty}^{+\infty} y_{ij}(t)u_i^*(t - \tau_{ij})e^{-j2\pi f_{D_{ij}}(t-\tau_{ij})}\mathrm{d}t\right|^2 - \frac{1}{\sigma^2 + \sigma_n^2}\left|\int_{-\infty}^{+\infty} a_{y_{ij}}u_i^*(t - \tau_{ij})e^{-j2\pi f_{D_{ij}}(t-\tau_{ij})}\mathrm{d}t\right|^2 \\ &+ \frac{2}{\sigma^2 + \sigma_n^2}\Re\left[\int_{-\infty}^{+\infty} y_{ij}(t)u_i^*(t - \tau_{ij})e^{-j2\pi f_{D_{ij}}(t-\tau_{ij})}\mathrm{d}t \times a_{y_{ij}}^* u_i(t - \tau_{ij})e^{j2\pi f_{D_{ij}}(t-\tau_{ij})}\mathrm{d}t\right]\Bigg\} + \left(\frac{\sigma_n^2}{\sigma^2 + \sigma_n^2}\right)\end{aligned} \tag{9}$$

where $a_{y_{ij}}$ represents the mean of the received signal $y_{ij}(t)$, i.e., $a_{y_{ij}} = a_{ij}u_i(t-\tau_{ij})e^{j2\pi f_{D_{ij}}(t-\tau_{ij})}$. Then, the log-likelihood ratio can be expressed as

$$L_{ij}(y_{ij}(t)|\mathbf{c}) = \frac{\sigma^2}{\sigma^2+\sigma_n^2}\left|\int_{-\infty}^{+\infty} y_{ij}(t)u_i^*(t-\tau_{ij})e^{-j2\pi f_{D_{ij}}(t-\tau_{ij})}\mathrm{d}t\right|^2 - \frac{1}{\sigma^2+\sigma_n^2}\left|\int_{-\infty}^{+\infty} a_{y_{ij}}u_i^*(t-\tau_{ij})e^{-j2\pi f_{D_{ij}}(t-\tau_{ij})}\mathrm{d}t\right|^2 + \frac{2}{\sigma^2+\sigma_n^2}\Re\left\{\int_{-\infty}^{+\infty} y_{ij}(t)u_i^*(t-\tau_{ij})e^{-j2\pi f_{D_{ij}}(t-\tau_{ij})}\mathrm{d}t \times a_{y_{ij}}^* u_i(t-\tau_{ij})e^{j2\pi f_{D_{ij}}(t-\tau_{ij})}\mathrm{d}t\right\} + \ln\left(\frac{\sigma_n^2}{\sigma^2+\sigma_n^2}\right) \tag{10}$$

Note that $y_{ij}(t)$ are mutually independent for different transmitter-receiver pairs due to the fact that the transmitters of opportunity and radar receivers are widely separated. Hence, the joint log-likelihood ratio across all the transmitter-receiver pairs can be written as the sum of the individual log-likelihood ratios:

$$L(\mathbf{y}(t)|\mathbf{c}) = \sum_{i=1}^{N_t}\sum_{j=1}^{N_r} L_{ij}(y_{ij}(t)|\mathbf{c}), \tag{11}$$

where

$$\mathbf{y}(t) = \left[y_{11}(t), y_{12}(t), \ldots, y_{N_tN_r}(t)\right]^\dagger \tag{12}$$

is the observed signals from the entire set of the receivers.

The CRLB indicates the smallest variance estimate of any unbiased estimate [*Filip and Shutin*, 2016; *Gogineni et al.*, 2014a; *He et al.*, 2010b], which can be utilized as a performance metric in parameter estimation problems due to the fact that the CRLB is close to the MSE of the MLE when the high signal-to-noise ratio (SNR) is satisfied. In the classical CRLB, the joint probability density function of the received signal and the parameter vector is utilized, while in MCRLB the expectation is taken on the conditional probability density function of the received signal conditioned on the transmitted symbols [*Javed et al.*, 2016]. Since the transmitted symbols c_{kl} are random, it is not feasible to calculate the classical CRLB in our study. Hence, the MCRLB is employed as a good alternative method by averaging the MFIM over the conditional probability density function of the received signal conditioned on the transmitted symbols, which shows a much looser bound than the classical CRLB in realistic scenarios. In this paper, we will compute the MCRLB for the joint position and velocity estimation of a Rician target in a OFDM-based passive radar network.

Given this statistical model, the MFIM is a 4×4 matrix related to the second-order derivatives of the joint log-likelihood function:

$$\begin{aligned}\mathbf{J}(\boldsymbol{\Theta}) &= \left(\nabla_{\boldsymbol{\Theta}}\boldsymbol{\Psi}^\dagger\right)\mathbf{J}(\boldsymbol{\Psi})\left(\nabla_{\boldsymbol{\Theta}}\boldsymbol{\Psi}^\dagger\right)^\dagger \\ &= \left(\nabla_{\boldsymbol{\Theta}}\boldsymbol{\Psi}^\dagger\right)\left(-\mathbb{E}_{\mathbf{y}(t)|\mathbf{c}}\left\{\nabla_{\boldsymbol{\Psi}}\left[\nabla_{\boldsymbol{\Psi}}L(\mathbf{y}(t)|\mathbf{c})\right]^\dagger\right\}\right)\left(\nabla_{\boldsymbol{\Theta}}\boldsymbol{\Psi}^\dagger\right)^\dagger,\end{aligned} \tag{13}$$

where $\boldsymbol{\Psi}$ is an alternative representation of the unknown parameter vector defined as

$$\boldsymbol{\Psi} = \left[\tau_{ij}, f_{D_{ij}}\right]^\dagger (\forall i, j). \tag{14}$$

We first derive $(\nabla_{\boldsymbol{\Theta}}\boldsymbol{\Psi}^\dagger)$ that corresponds to the change of variables. The derivatives of the time delays with respect to the target positions can be obtained as

$$\frac{\partial\tau_{ij}}{\partial x} \equiv \frac{1}{c}\left(\frac{x-x_i^t}{\left\|\vec{\mathbf{p}}-\vec{\mathbf{p}}_i^t\right\|} + \frac{x-x_j^r}{\left\|\vec{\mathbf{p}}-\vec{\mathbf{p}}_j^r\right\|}\right), \tag{15}$$

$$\frac{\partial\tau_{ij}}{\partial y} \equiv \frac{1}{c}\left(\frac{y-y_i^t}{\left\|\vec{\mathbf{p}}-\vec{\mathbf{p}}_i^t\right\|} + \frac{y-y_j^r}{\left\|\vec{\mathbf{p}}-\vec{\mathbf{p}}_j^r\right\|}\right). \tag{16}$$

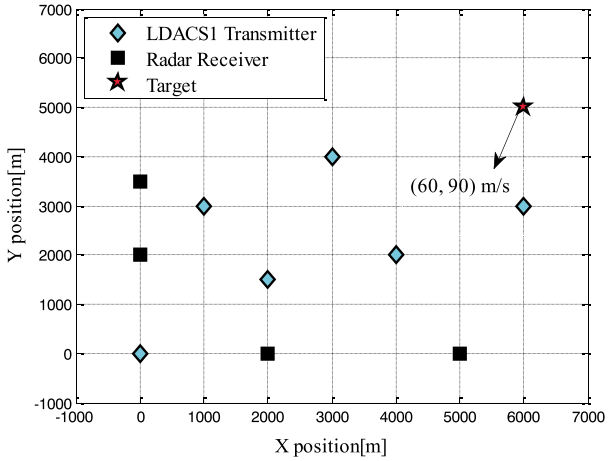

Figure 1. Target and the passive radar networks configuration used in the numerical simulations.

The derivatives of the time delays with respect to the target velocities are

$$\frac{\partial \tau_{ij}}{\partial v_x} \equiv 0, \tag{17}$$

$$\frac{\partial \tau_{ij}}{\partial v_y} \equiv 0. \tag{18}$$

Similarly, the derivatives of the Doppler shifts with respect to the target positions can be given by

$$\frac{\partial f_{D_{ij}}}{\partial x} \equiv \frac{f_c}{c}\left\{v_x\left[\frac{\left(y-y_i^t\right)^2}{\left\|\vec{\mathbf{p}}-\vec{\mathbf{p}}_i^t\right\|^3}+\frac{\left(y-y_j^r\right)^2}{\left\|\vec{\mathbf{p}}-\vec{\mathbf{p}}_j^r\right\|^3}\right]+v_y\left[-\frac{\left(x-x_i^t\right)\left(y-y_j^r\right)}{\left\|\vec{\mathbf{p}}-\vec{\mathbf{p}}_i^t\right\|^3}-\frac{\left(x-x_j^r\right)\left(y-y_j^r\right)}{\left\|\vec{\mathbf{p}}-\vec{\mathbf{p}}_j^r\right\|^3}\right]\right.$$
$$\left.+\left[v_{x,j}^r\frac{\left(y-y_j^r\right)^2}{\|\vec{\mathbf{p}}-\vec{\mathbf{p}}_j^r\|^3}-v_{y,j}^r\frac{\left(x-x_j^r\right)\left(y-y_j^r\right)}{\|\vec{\mathbf{p}}-\vec{\mathbf{p}}_j^r\|^3}\right]\right\}, \tag{19}$$

$$\frac{\partial f_{D_{ij}}}{\partial y} \equiv \frac{f_c}{c}\left\{v_y\left[\frac{\left(x-x_i^t\right)^2}{\left\|\vec{\mathbf{p}}-\vec{\mathbf{p}}_i^t\right\|^3}+\frac{\left(x-x_j^r\right)^2}{\left\|\vec{\mathbf{p}}-\vec{\mathbf{p}}_j^r\right\|^3}\right]+v_x\left[-\frac{\left(x-x_i^t\right)\left(y-y_j^r\right)}{\left\|\vec{\mathbf{p}}-\vec{\mathbf{p}}_i^t\right\|^3}-\frac{\left(x-x_j^r\right)\left(y-y_j^r\right)}{\left\|\vec{\mathbf{p}}-\vec{\mathbf{p}}_j^r\right\|^3}\right]\right.$$
$$\left.+\left[-v_{x,j}^r\frac{\left(x-x_j^r\right)\left(y-y_j^r\right)}{\|\vec{\mathbf{p}}-\vec{\mathbf{p}}_j^r\|^3}+v_{y,j}^r\frac{\left(x-x_j^r\right)^2}{\|\vec{\mathbf{p}}-\vec{\mathbf{p}}_j^r\|^3}\right]\right\}, \tag{20}$$

Table 1. Transmitters of Opportunity Positions

Transmitter	Position (m)
1	[0, 0]
2	[2000, 1500]
3	[4000, 2000]
4	[3000, 4000]
5	[1000, 3000]
6	[6000, 3000]

Table 2. Multichannel Receivers Positions and Velocities

Receiver	Position (m)	Velocity (m/s)
1	[2000, 0]	[30, 50]
2	[5000, 0]	[10, 70]
3	[0, 2000]	[60, 50]
4	[0, 3500]	[80, 20]

and the derivatives of the Doppler shifts with respect to the target velocities are obtained as

$$\frac{\partial f_{D_{ij}}}{\partial v_x} \equiv \frac{f_c}{c}\left(\frac{x - x_i^t}{\left\|\vec{\mathbf{p}} - \vec{\mathbf{p}}_i^t\right\|} + \frac{x - x_j^r}{\left\|\vec{\mathbf{p}} - \vec{\mathbf{p}}_j^r\right\|}\right), \tag{21}$$

$$\frac{\partial f_{D_{ij}}}{\partial v_y} \equiv \frac{f_c}{c}\left(\frac{y - y_i^t}{\left\|\vec{\mathbf{p}} - \vec{\mathbf{p}}_i^t\right\|} + \frac{y - y_j^r}{\left\|\vec{\mathbf{p}} - \vec{\mathbf{p}}_j^r\right\|}\right), \tag{22}$$

where the derivatives of (19) and (20) are provided in Appendix A.

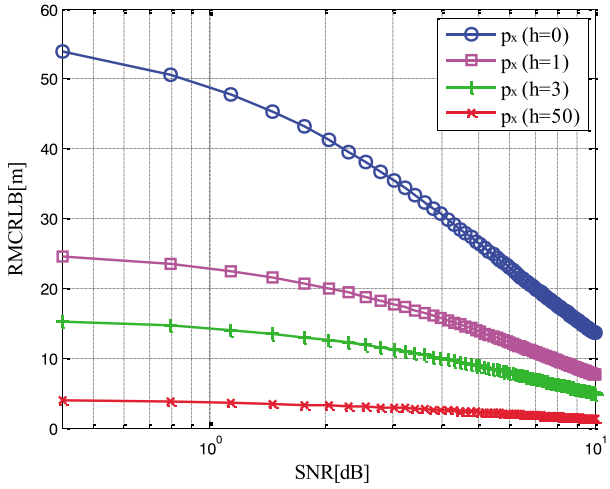

Figure 2. RMCRLB in the target position dimensions versus SNR with different *h*: (a) *x* position dimension; (b) *y* position dimension.

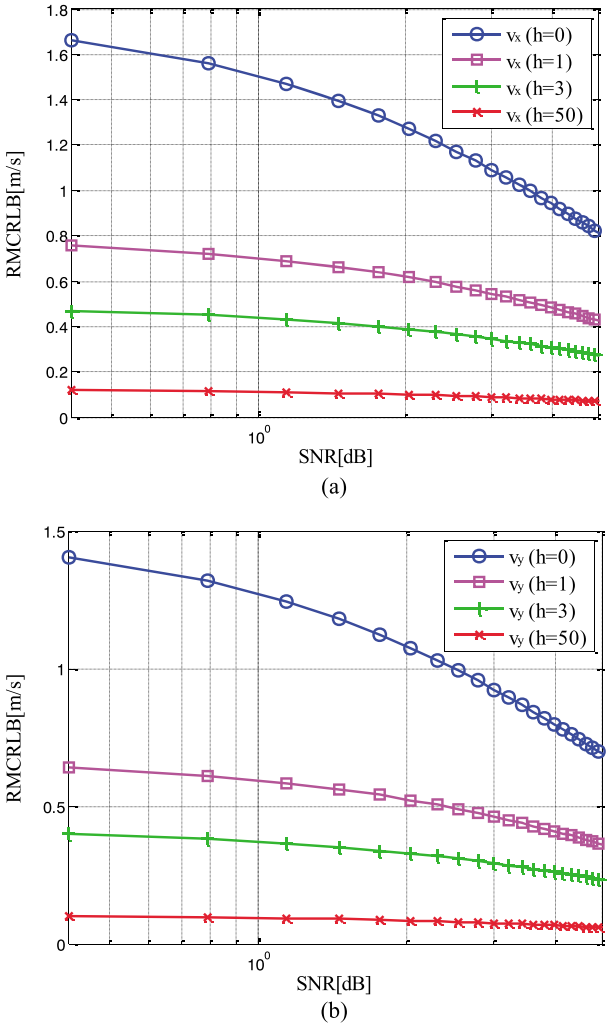

Figure 3. RMCRLB in the target velocity dimensions versus SNR with different *h*: (a) *x* velocity dimension; (b) *y* velocity dimension.

After lengthy algebraic derivations, the closed-form expression of the total MFIM $\mathbf{J}(\mathbf{\Psi})$ over all the transmitter-receiver pairs is given as

$$\begin{aligned}\mathbf{J}(\mathbf{\Psi}) &= -\mathbb{E}_{\mathbf{y}(t)|\mathbf{c}}\left\{\nabla_{\mathbf{\Psi}} L(\mathbf{y}(t)|\mathbf{c})[\nabla_{\mathbf{\Psi}} L(\mathbf{y}(t)|\mathbf{c})]^{\dagger}\right\} = -\mathbb{E}_{\mathbf{y}(t)|\mathbf{c}}\left\{\nabla_{\mathbf{\Psi}}[\nabla_{\mathbf{\Psi}} L(\mathbf{y}(t)|\mathbf{c})]^{\dagger}\right\} \\ &= \sum_{i=1}^{N_t}\sum_{j=1}^{N_r} \frac{8\pi^2\sigma^4}{\sigma_n^2\left(\sigma^2+\sigma_n^2\right)}\left[1+2h_{ij}+\frac{2h_{ij}}{\left(\sigma^2/\sigma_n^2\right)}\right]\times\begin{bmatrix}\varepsilon_i & 0\\ 0 & \eta_{ij}\end{bmatrix},\end{aligned} \tag{23}$$

where the terms ε_i and η_{ij} are dependent on the transmitted signals, which are computed as follows [*Filip and Shutin*, 2016]:

$$\begin{aligned}\varepsilon_i &\equiv \mathbb{E}\left\{\int_{-\infty}^{+\infty} f^2\left|U_i(f)\right|^2 \mathrm{d}f - \left|\int_{-\infty}^{+\infty} f\left|U_i(f)\right|^2 \mathrm{d}f\right|^2\right\} \\ &= \frac{3+\Delta f^2 T_{\mathrm{w}}(4T_{\mathrm{s}}-T_{\mathrm{w}})(N_{\mathrm{u}}^2-1)}{12T_{\mathrm{w}}(4T_{\mathrm{s}}-T_{\mathrm{w}})},\end{aligned} \tag{24}$$

$$\begin{aligned}\eta_{ij} &\equiv \mathbb{E}\left\{\int_{-\infty}^{+\infty} t^2\left|u_i(t)\right|^2 \mathrm{d}f - \left|\int_{-\infty}^{+\infty} t\left|u_i(t)\right|^2 \mathrm{d}f\right|^2\right\} \\ &= \frac{4\pi^2L^2T_{\mathrm{s}}^3-\pi^2(L^2+2)T_{\mathrm{s}}^2T_{\mathrm{w}}-(\pi^2-6)T_{\mathrm{w}}^3}{12\pi^2(4T_{\mathrm{s}}-T_{\mathrm{w}})}+\frac{(\pi^2-8)T_{\mathrm{s}}T_{\mathrm{w}}^2}{\pi^2(4T_{\mathrm{s}}-T_{\mathrm{w}})}.\end{aligned} \tag{25}$$

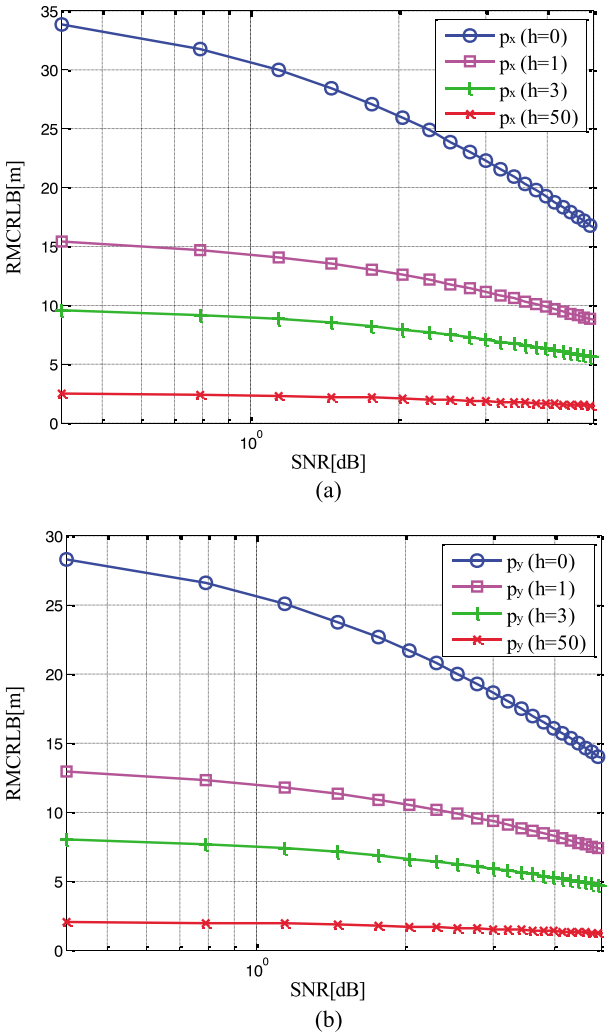

Figure 4. RMCRLB in the target position dimensions versus SNR with different h when $[x, y] = [3000, 5000]$ m: (a) x position dimension; (b) y position dimension.

The derivation of $\mathbf{J}(\mathbf{\Psi})$ in (23) is given in Appendix B. The analysis in *Filip and Shutin*. [2016] expresses the MFIM as a combination of the constituent bistatic FIMs. Therefore, we can write the MFIM for OFDM-based passive radar networks as follows:

$$\mathbf{J}(\mathbf{\Theta}) = \sum_{i=1}^{N_t}\sum_{j=1}^{N_r} \frac{8\pi^2\sigma^4}{\sigma_n^2\left(\sigma^2+\sigma_n^2\right)}\left(1+2h_{ij}+\frac{2h_{ij}}{\left(\sigma^2/\sigma_n^2\right)}\right)\mathbf{J}_{ij}(\mathbf{\Theta}), \tag{26}$$

where $h_{ij} = |a_{ij}|^2/(2\sigma^2)$. The final expressions for the elements of the bistatic MFIM $\mathbf{J}_{ij}(\mathbf{\Theta})$ corresponding to the ijth transmitter-receiver pair are shown in Appendix C. It can be observed from (26) that the MFIM is a linear combination of the components contributing from DS and WIS, which can be factored into two terms: one term accounting for the effect of the DS component and another term incorporating the effect of the WIS component. Define the SNR as

$$\mathrm{SNR} = \frac{\sigma^2}{\sigma_n^2}. \tag{27}$$

Then, the MFIM in (26) can be rewritten as follows:

$$\mathbf{J}(\mathbf{\Theta}) = \sum_{i=1}^{N_t}\sum_{j=1}^{N_r} \frac{8\pi^2\mathrm{SNR}^2}{1+\mathrm{SNR}}\left(1+2h_{ij}+\frac{2h_{ij}}{\mathrm{SNR}}\right)\mathbf{J}_{ij}(\mathbf{\Theta}). \tag{28}$$

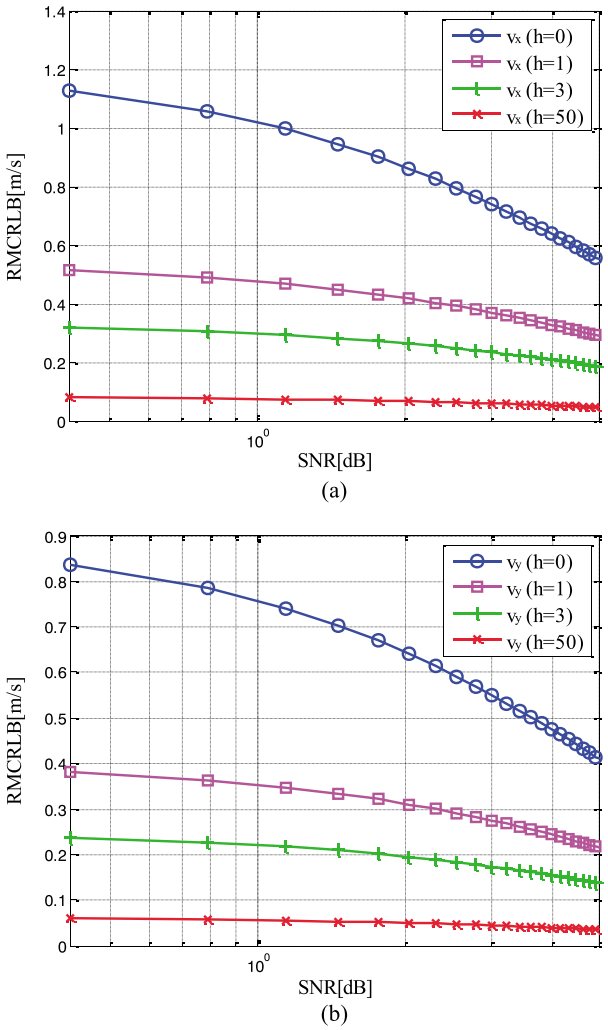

Figure 5. RMCRLB in the target velocity dimensions versus SNR with different h when $[x, y] = [3000, 5000]$ m: (a) x velocity dimension; (b) y velocity dimension.

The MCRLB matrix for the joint estimation of a Rician target position and velocity can be obtained by taking the inverse of MFIM in (28) as

$$\mathrm{MCRLB}(\boldsymbol{\Theta}) = \mathbf{J}^{-1}(\boldsymbol{\Theta}). \tag{29}$$

Furthermore, the joint MCRLBs for the estimation of target position and velocity are determined by the four diagonal elements of the MCRLB matrix such that

$$\begin{cases} \mathrm{MCRLB}^{x}(\boldsymbol{\Theta}) = \left[\mathbf{J}^{-1}(\boldsymbol{\Theta})\right]_{1,1}, \mathrm{MCRLB}^{y}(\boldsymbol{\Theta}) = \left[\mathbf{J}^{-1}(\boldsymbol{\Theta})\right]_{2,2}, \\ \mathrm{MCRLB}^{v_x}(\boldsymbol{\Theta}) = \left[\mathbf{J}^{-1}(\boldsymbol{\Theta})\right]_{3,3}, \mathrm{MCRLB}^{v_y}(\boldsymbol{\Theta}) = \left[\mathbf{J}^{-1}(\boldsymbol{\Theta})\right]_{4,4}. \end{cases} \tag{30}$$

Remark 1: It can be observed from (30) that the MCRLB depends on several factors. It not only depends on the relative geometry between the target and the passive radar network system but also depends on the transmitted waveform parameters such as symbol duration and the number of OFDM symbols. In addition, it shows dependence on the target's RCS and the SNR.

Remark 2: As indicated in *Javed et al*. [2016], we can adopt $h'_{ij} = h_{ij}/(1 + h_{ij})$ for the categorization of the Swerling RCS models. Specifically, $h'_{ij} = 0$, 0.75, and 1 correspond to the Swerling I/II models, Swerling III/IV models, and Swerling 0/V models, respectively. In addition, $h'_{ij} = 0$ indicates that the target RCS with WIS component follows Rayleigh fluctuations in a noncoherent mode for all the transmitter-receiver pairs,

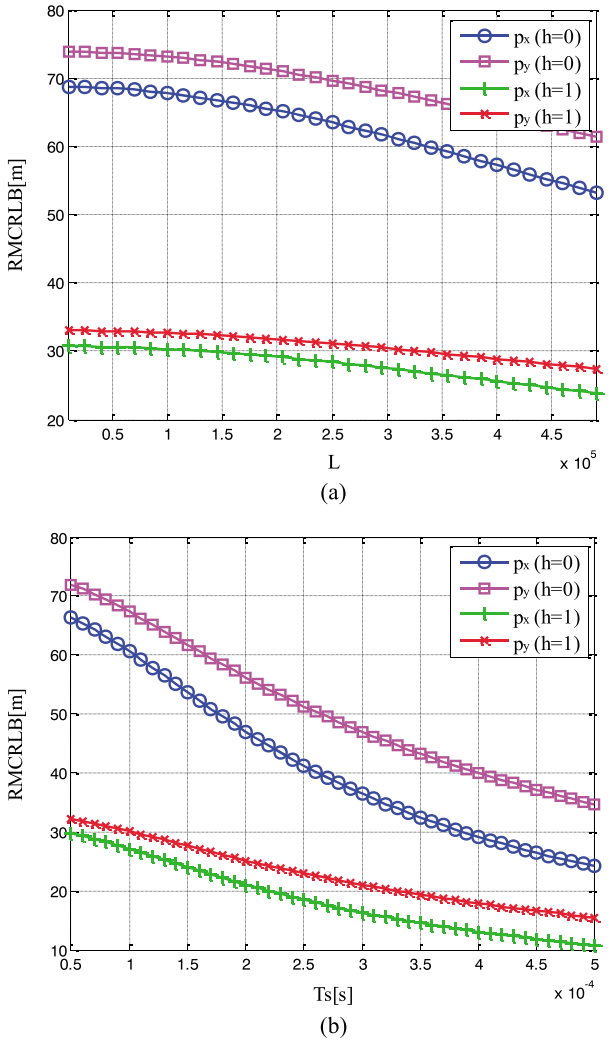

Figure 6. RMCRLB in the target position dimensions versus waveform parameters when SNR = 0 dB with different *h*: (a) *L*; (b) T_s.

whereas h'_{ij}=1 means that the target is a point target in a coherent mode, which has a fixed amplitude RCS value for all the transmitter-receiver pairs.

4. Numerical Simulations and Analysis

In the following, some numerical simulation results are provided to verify the accuracy of the theoretical derivations and reveal the effects of several factors on the MCRLBs.

4.1. Description

In this paper, we consider a passive radar network with $N_t = 6$ OFDM-based LDACS1 transmitters of opportunity and N_r=4 multichannel receivers. The passive radar network architecture studied here and the corresponding geometry between the target and the passive radar network system are depicted in Figure 1.

The positions of the transmitters are given in Table 1. The positions and velocities of the radar receivers are given in Table 2. The target moving with *x-y* velocity [60, 90] m/s is located at [6000, 5000] m. We choose the same OFDM signal parameters as in *Javed et al*. [2016] for the simulations: the total number of subcarriers $N_u = 64$, the subcarrier spacing $\Delta f = 9.7$ kHz, the total symbol duration $T_s = 120\,\mu$s, the windowing duration $T_w = 12.8\,\mu$s, the number of OFDM symbols $L = 384620$, and the carrier frequency $f_c = 971.5$ kHz.

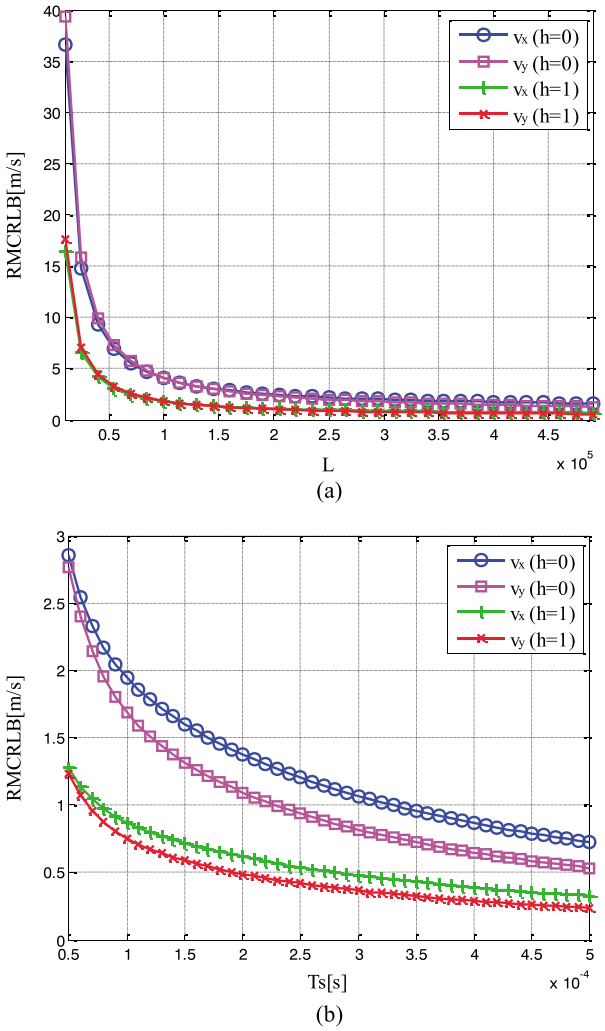

Figure 7. RMCRLB in the target velocity dimensions versus waveform parameters when SNR = 0 dB with different h: (a) L; (b) T_s.

4.2. Numerical Results

Herein, without loss of generality, we assume that h_{ij} is the same for all transmitter-receiver pairs, i.e., $h_{ij} = h$. It can be observed in Figure 2 the curves of the square root of MCRLB (RMCRLB) in the x position and y position dimensions versus SNR with different h. Similarly, it is depicted in Figure 3 that the velocity RMCRLB is a function of the varying SNR. These figures show that the values of RMCRLB reduce as the SNR increases, where it can be seen that the RMCRLBs in the y dimension are greater than those in the x dimension for the position, while the RMCRLBs is lower in the y dimension for the velocity.

Moreover, it is apparent from Figures 2 and 3 that as the value of h increases, the RMCRLBs decrease for both the target position and velocity estimates, which is due to the fact that the increase in h provides a rise in target RCS [*Javed et al*., 2016]. Consequently, the SNR goes up at the radar receiver. The RMCRLB will achieve a maximum value when DS component does not exist, i.e., $h = 0$, where the target RCS follows Rayleigh fluctuations in a noncoherent mode for all the transmitter-receiver pairs. In contrast, the RMCRLB will be minimum at an asymptotic limit, i.e., $h \to \infty$, and the target is idealistically a point target in a coherent mode, which has a fixed amplitude RCS value for all the transmitter-receiver pairs. For the rest of the other cases, the RMCRLB lies in between these two values.

Furthermore, in order to examine the effect of the relative geometry between the target and the passive radar network systems on the RMCRLB, we change the target position to [3000, 5000] m. It is evident from Figure 4 that the RMCRLBs are different from the earlier case. This is because the relative geometry between

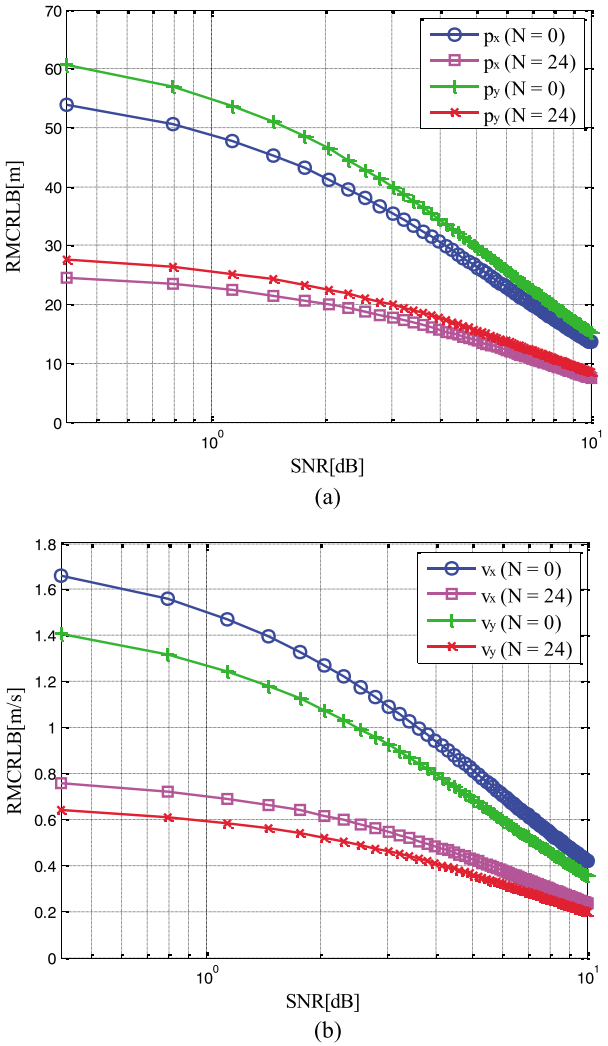

Figure 8. RMCRLB versus SNR with different number of transmitter-receiver pairs with DS component: (a) target position dimension; (b) target velocity dimension.

the moving target and the OFDM-based passive radar networks has a significant effect on the derivatives of Ψ in (13) [*Gogineni et al*., 2014; *Shi et al*., 2016a]. In Figure 4, it can be noticed that the values of RMCRLBs for target position are decreased as the SNR goes up. To be specific, the RCRLB at 1.65 dB is 45.3 m for *x* dimension and 50.98 m for *y* dimension in Figure 2. As the geometry between the target and the radar networks changes, the RCRLB values are changed and become 28.39 m for *x* dimension and 23.74 m for *y* dimension in Figure 4. Also, the RMCRLBs are larger in the *x* dimension than those in the *y* dimension, which is different from the case when the true target position was [6000, 5000] m. In addition, as we can see in Figure 5, the values are different from the earlier case and the same holds true for the target velocity RMCRLBs. Specifically, in Figure 3, the RCRLB at 3.1 dB is 1.271 m/s for *x* dimension and 1.075 m/s for *y* dimension, while the RCRLBs are changed in Figure 5 and become 0.861 m/s for *x* dimension and 0.6404 m/s for *y* dimension.

In Figures 6 and 7, the RMCRLBs for target position and velocity dimensions are plotted against the waveform parameters when SNR $=$ 0 dB with different *h*. Specifically, how the number of transmitted OFDM symbols *L* and the total symbol duration T_s impact the joint estimation performance is described exactly. We can observe from Figures 6 and 7 that the RMCRLBs decrease with the increase of the waveform parameters, which confirms that a waveform with a larger data set can provide better target parameter estimation accuracy. Therefore, we can conclude that the joint MCRLB is a function of the transmitted waveform parameters as well as the geometry between the target and the passive radar networks, the target's RCS and SNR.

Figure 8 illustrates the RMCRLBs for target position and velocity dimensions versus SNR with different number of transmitter-receiver pairs with DS component, i.e., *N*. One can see that the RMCRLBs are reduced as the number of transmitter-receiver pairs with DS component goes up, which confirms that the number of the DS components has significant effect on the target parameter estimation performance.

5. Conclusion

In a realistic scenario, the Rician target with both the DS and WIS components is more favorable than the Rayleigh target only with WIS component. This is because the Rician model is practical and can be utilized to approximate a broad range of Swerling 0-V target models. In this study, we investigated the problem of joint position and velocity estimation of a Rician target in OFDM-based passive radar networks with multichannel receivers on moving platforms, which consist of multiple OFDM-based LDACS1 transmitters of opportunity and multiple radar receivers. The joint MCRLB on the Cartesian coordinates of target position and velocity in a Rice fading environment has been computed. It is shown in numerical simulation results that the joint target parameter estimation accuracy of the passive radar networks can be significantly improved with the exploitation of the DS component. Furthermore, it is worth pointing out that the joint MCRLB is a function not only of the transmitted waveform parameters but also of the relative geometry, which incorporates the positions of the transmitters, receivers, and the target in a Cartesian space. Also, it shows dependence on the target RCS and SNR. Note that only single target is considered in this paper. However, the model and derivations can be extended to a multiple targets scenario, and the conclusions obtained in this study suggest that similar results would be achieved for the multiple targets case. Future work will focus on the problem of optimal transmitter-receiver pair selection for the OFDM-based passive radar network systems.

Appendix A: The Derivation of (19) and (20)

Here, we derive the derivatives of the Doppler terms with respect to the target positions (19) and (20) by utilizing Doppler shift (7). As we have

$$\frac{\partial\left[v_x\left(\frac{x-x_i^t}{\left\|\vec{\mathbf{p}}-\vec{\mathbf{p}}_i^t\right\|}\right)\right]}{\partial x}=v_x\frac{\left\|\vec{\mathbf{p}}-\vec{\mathbf{p}}_i^t\right\|-\left(x-x_i^t\right)\frac{x-x_i^t}{\left\|\vec{\mathbf{p}}-\vec{\mathbf{p}}_i^t\right\|}}{\left\|\vec{\mathbf{p}}-\vec{\mathbf{p}}_i^t\right\|^2}=v_x\frac{\left(y-y_i^t\right)^2}{\left\|\vec{\mathbf{p}}-\vec{\mathbf{p}}_i^t\right\|^3}, \tag{A1}$$

$$\frac{\partial\left[v_x\left(\frac{x-x_j^r}{\left\|\vec{\mathbf{p}}-\vec{\mathbf{p}}_j^r\right\|}\right)\right]}{\partial x}=v_x\frac{\left\|\vec{\mathbf{p}}-\vec{\mathbf{p}}_j^r\right\|-\left(x-x_j^r\right)\frac{x-x_j^r}{\left\|\vec{\mathbf{p}}-\vec{\mathbf{p}}_j^r\right\|}}{\left\|\vec{\mathbf{p}}-\vec{\mathbf{p}}_j^r\right\|^2}=v_x\frac{\left(y-y_j^r\right)^2}{\left\|\vec{\mathbf{p}}-\vec{\mathbf{p}}_j^r\right\|^3}, \tag{A2}$$

$$\frac{\partial\left[v_y\left(\frac{y-y_i^t}{\left\|\vec{\mathbf{p}}-\vec{\mathbf{p}}_i^t\right\|}\right)\right]}{\partial x}=v_y\frac{-(y-y_{r,j})\frac{(x-x_t)}{\left\|\vec{\mathbf{p}}-\vec{\mathbf{p}}_i^t\right\|}}{\left\|\vec{\mathbf{p}}-\vec{\mathbf{p}}_i^t\right\|^2}=-v_y\frac{\left(x-x_i^t\right)\left(y-y_j^r\right)}{\left\|\vec{\mathbf{p}}-\vec{\mathbf{p}}_i^t\right\|^3}, \tag{A3}$$

$$\frac{\partial\left[v_y\left(\frac{y-y_j^r}{\left\|\vec{\mathbf{p}}-\vec{\mathbf{p}}_j^r\right\|}\right)\right]}{\partial x}=-v_y\frac{\left(x-x_j^r\right)\left(y-y_j^r\right)}{\left\|\vec{\mathbf{p}}-\vec{\mathbf{p}}_j^r\right\|^3}, \tag{A4}$$

$$\frac{\partial\left[v_{x,j}^r\left(\frac{x-x_j^r}{\left\|\vec{\mathbf{p}}-\vec{\mathbf{p}}_j^r\right\|}\right)\right]}{\partial x}=v_{x,j}^r\frac{\left(y-y_j^r\right)^2}{\left\|\vec{\mathbf{p}}-\vec{\mathbf{p}}_j^r\right\|^3}, \tag{A5}$$

$$\frac{\partial\left[v_{y,j}^{r}\left(\frac{y-y_j^r}{\left\|\vec{\mathbf{p}}-\vec{\mathbf{p}}_j^r\right\|}\right)\right]}{\partial x}=-v_{y,j}^{r}\frac{\left(x-x_j^r\right)\left(y-y_j^r\right)}{\left\|\vec{\mathbf{p}}-\vec{\mathbf{p}}_j^r\right\|^3}. \tag{A6}$$

Hence, the derivative of the Doppler term with respect to the target position x can be obtained as follows:

$$\begin{aligned}\frac{\partial f_{D_{ij}}}{\partial x}\equiv\frac{f_c}{c}\Bigg\{&v_x\left[\frac{\left(y-y_i^t\right)^2}{\left\|\vec{\mathbf{p}}-\vec{\mathbf{p}}_i^t\right\|^3}+\frac{\left(y-y_j^r\right)^2}{\left\|\vec{\mathbf{p}}-\vec{\mathbf{p}}_j^r\right\|^3}\right]\\&+v_y\left[-\frac{\left(x-x_i^t\right)\left(y-y_j^r\right)}{\left\|\vec{\mathbf{p}}-\vec{\mathbf{p}}_i^t\right\|^3}-\frac{\left(x-x_j^r\right)\left(y-y_j^r\right)}{\left\|\vec{\mathbf{p}}-\vec{\mathbf{p}}_j^r\right\|^3}\right]\\&+\left[v_{x,j}^{r}\frac{\left(y-y_j^r\right)^2}{\|\vec{\mathbf{p}}-\vec{\mathbf{p}}_j^r\|^3}-v_{y,j}^{r}\frac{\left(x-x_j^r\right)\left(y-y_j^r\right)}{\|\vec{\mathbf{p}}-\vec{\mathbf{p}}_j^r\|^3}\right]\Bigg\}.\end{aligned} \tag{A7}$$

Similarly, the derivative of the Doppler term with respect to the Cartesian position y is calculated as

$$\frac{\partial\left[v_x\left(\frac{x-x_i^t}{\left\|\vec{\mathbf{p}}-\vec{\mathbf{p}}_i^t\right\|}\right)\right]}{\partial y}=-v_x\frac{\left(x-x_i^t\right)\left(y-y_j^r\right)}{\left\|\vec{\mathbf{p}}-\vec{\mathbf{p}}_i^t\right\|^3}, \tag{A8}$$

$$\frac{\partial\left[v_x\left(\frac{x-x_j^r}{\left\|\vec{\mathbf{p}}-\vec{\mathbf{p}}_j^r\right\|}\right)\right]}{\partial y}=-v_x\frac{\left(x-x_j^r\right)\left(y-y_j^r\right)}{\left\|\vec{\mathbf{p}}-\vec{\mathbf{p}}_j^r\right\|^3}, \tag{A9}$$

$$\frac{\partial\left[v_y\left(\frac{y-y_i^t}{\left\|\vec{\mathbf{p}}-\vec{\mathbf{p}}_i^t\right\|}\right)\right]}{\partial y}=v_y\frac{\left\|\vec{\mathbf{p}}-\vec{\mathbf{p}}_i^t\right\|-\left(y-y_i^t\right)\frac{y-y_i^t}{\left\|\vec{\mathbf{p}}-\vec{\mathbf{p}}_i^t\right\|}}{\left\|\vec{\mathbf{p}}-\vec{\mathbf{p}}_i^t\right\|^2}=v_y\frac{\left(x-x_i^t\right)^2}{\left\|\vec{\mathbf{p}}-\vec{\mathbf{p}}_i^t\right\|^3}, \tag{A10}$$

$$\frac{\partial\left[v_y\left(\frac{y-y_j^r}{\left\|\vec{\mathbf{p}}-\vec{\mathbf{p}}_j^r\right\|}\right)\right]}{\partial y}=v_y\frac{\left\|\vec{\mathbf{p}}-\vec{\mathbf{p}}_j^r\right\|-\left(y-y_j^r\right)\frac{y-y_j^r}{\left\|\vec{\mathbf{p}}-\vec{\mathbf{p}}_j^r\right\|}}{\left\|\vec{\mathbf{p}}-\vec{\mathbf{p}}_j^r\right\|^2}=v_y\frac{\left(x-x_j^r\right)^2}{\left\|\vec{\mathbf{p}}-\vec{\mathbf{p}}_j^r\right\|^3}, \tag{A11}$$

$$\frac{\partial\left[v_{x,j}^{r}\left(\frac{x-x_j^r}{\left\|\vec{\mathbf{p}}-\vec{\mathbf{p}}_j^r\right\|}\right)\right]}{\partial y}=-v_{x,j}^{r}\frac{\left(x-x_j^r\right)\left(y-y_j^r\right)}{\left\|\vec{\mathbf{p}}-\vec{\mathbf{p}}_j^r\right\|^3}, \tag{A12}$$

$$\frac{\partial\left[v_{y,j}^{r}\left(\frac{y-y_j^r}{\left\|\vec{\mathbf{p}}-\vec{\mathbf{p}}_j^r\right\|}\right)\right]}{\partial y}=v_{y,j}^{r}\frac{\left\|\vec{\mathbf{p}}-\vec{\mathbf{p}}_j^r\right\|-\left(y-y_j^r\right)\frac{y-y_j^r}{\left\|\vec{\mathbf{p}}-\vec{\mathbf{p}}_j^r\right\|}}{\|\vec{\mathbf{p}}-\vec{\mathbf{p}}_j^r\|^2}=v_{y,j}^{r}\frac{\left(x-x_j^r\right)^2}{\left\|\vec{\mathbf{p}}-\vec{\mathbf{p}}_j^r\right\|^3}. \tag{A13}$$

Therefore, we have

$$\frac{\partial f_{D_{ij}}}{\partial y} \equiv \frac{f_c}{c}\left\{ v_y \left[\frac{\left(x - x_i^t\right)^2}{\left\|\vec{\mathbf{p}} - \vec{\mathbf{p}}_i^t\right\|^3} + \frac{\left(x - x_j^r\right)^2}{\left\|\vec{\mathbf{p}} - \vec{\mathbf{p}}_j^r\right\|^3} \right] + v_x \left[-\frac{\left(x - x_i^t\right)\left(y - y_j^r\right)}{\left\|\vec{\mathbf{p}} - \vec{\mathbf{p}}_i^t\right\|^3} - \frac{\left(x - x_j^r\right)\left(y - y_j^r\right)}{\left\|\vec{\mathbf{p}} - \vec{\mathbf{p}}_j^r\right\|^3} \right] + \left[-v_{x,j}^r \frac{\left(x - x_j^r\right)\left(y - y_j^r\right)}{\|\vec{\mathbf{p}} - \vec{\mathbf{p}}_j^r\|^3} + v_{y,j}^r \frac{\left(x - x_j^r\right)^2}{\|\vec{\mathbf{p}} - \vec{\mathbf{p}}_j^r\|^3} \right] \right\}. \tag{A14}$$

Appendix B: The Derivation of J(Ψ)

Here, we derive the closed-form expressions for the elements of the MFIM matrix $\mathbf{J}(\boldsymbol{\Psi})$. From (10) and (11), we have

$$\begin{aligned} L(\mathbf{y}(t)|\mathbf{c}) &= \sum_{i=1}^{N_t}\sum_{j=1}^{N_r} L_{ij}(y_{ij}(t)|\mathbf{c}) \\ &= \sum_{i=1}^{N_t}\sum_{j=1}^{N_r}\left(T_{ij}^1 - T_{ij}^2 + T_{ij}^3\right) + C, \end{aligned} \tag{B1}$$

where T_{ij}^1, T_{ij}^2 and T_{ij}^3 represent the first, second, and third terms in (11), respectively. Then, we can obtain

$$T_{ij}^1 = \frac{\sigma^2}{\sigma^2 + \sigma_n^2}\left| \int_{-\infty}^{+\infty} y_{ij}(t) u_i^*(t - \tau_{ij}) e^{-j2\pi f_{D_{ij}}(t-\tau_{ij})} \mathrm{d}t \right|^2. \tag{B2}$$

Let us suppose $\delta_{ij} = \int_{-\infty}^{+\infty} y_{ij}(t) u_i^*(t - \tau_{ij}) e^{-j2\pi f_{D_{ij}}(t-\tau_{ij})} \mathrm{d}t$, then the first derivative with respect to τ_{ij} is given by

$$\begin{aligned} \frac{\partial T_{ij}^1}{\partial \tau_{ij}} &= \frac{\sigma^2}{\sigma^2 + \sigma_n^2}\left(\delta_{ij}^* \frac{\partial \delta_{ij}}{\partial \tau_{ij}} + \delta_{ij} \frac{\partial \delta_{ij}^*}{\partial \tau_{ij}} \right) \\ &= \frac{2\sigma^2}{\sigma_n^2(\sigma^2 + \sigma_n^2)} \times \Re\left(\delta_{ij} \int_{-\infty}^{+\infty} y_{ij}^*(t) \frac{\partial u_i(t - \tau_{ij})}{\partial \tau_{ij}} e^{j2\pi f_{D_{ij}}(t-\tau_{ij})} \right) \end{aligned} \tag{B3}$$

To compute the expectation with respect to the second-order derivative, we have

$$\begin{aligned} -\mathbb{E}\left(\frac{\partial^2 T_{ij}^1}{\partial \tau_{ij}^2} \right) = -\frac{2\sigma^2\left(\sigma^2 + a_{ij}^2\right)}{\sigma^2 + \sigma_n^2} \times \mathbb{E}\left[\Re\left(\left| \int_{-\infty}^{+\infty} u_i(t - \tau_{ij}) \frac{\partial u_i^*(t - \tau_{ij})}{\partial \tau_{ij}} \mathrm{d}t \right|^2 \right.\right. \\ \left.\left. + \int_{-\infty}^{+\infty} |u_i(t - \tau_{ij})|^2 \mathrm{d}t \int_{-\infty}^{+\infty} u_i^*(t - \tau_{ij}) \frac{\partial^2 u_i(t - \tau_{ij})}{\partial \tau_{ij}^2} \mathrm{d}t \right) \right]. \end{aligned} \tag{B4}$$

With the derivations in *Filip and Shutin* [2016] and *Javed et al.* [2016], hence we obtain

$$-\mathbb{E}\left(\frac{\partial^2 T_{ij}^1}{\partial \tau_{ij}^2} \right) = \frac{8\pi^2\sigma^4}{\sigma_n^2\left(\sigma^2 + \sigma_n^2\right)}(1 + 2h_{ij})\epsilon_i, \tag{B5}$$

where $h_{ij} = |a_{ij}|^2/(2\sigma^2)$. To calculate the expectation with respect to other second-order derivatives, we follow the same procedure and arrive at the following closed-form expression:

$$-\mathbb{E}\left(\frac{\partial^2 T_{ij}^1}{\partial f_{D_{ij}}^2} \right) = \frac{8\pi^2\sigma^4}{\sigma_n^2\left(\sigma^2 + \sigma_n^2\right)}(1 + 2h_{ij})\eta_{ij}. \tag{B6}$$

The off-diagonal terms turn out to be zero in agreement with the derivations in (A4); that is,

$$-\mathbb{E}\left(\frac{\partial^2 T_{ij}^1}{\partial\tau_{ij}\partial f_{D_{ij}}}\right)=0. \tag{B7}$$

Following the same lines, we can get the expectation of second-order derivatives of T_{ij}^2 and T_{ij}^3 as follows:

$$-\mathbb{E}\left(\frac{\partial^2 T_{ij}^2}{\partial\tau_{ij}^2}\right)=\frac{8\pi^2\sigma^4}{\sigma_n^2\left(\sigma^2+\sigma_n^2\right)}\left(-\frac{2h_{ij}}{\sigma^2/\sigma_n^2}\right)\varepsilon_i, \tag{B8}$$

$$-\mathbb{E}\left(\frac{\partial^2 T_{ij}^2}{\partial f_{D_{ij}}^2}\right)=\frac{8\pi^2\sigma^4}{\sigma_n^2\left(\sigma^2+\sigma_n^2\right)}\left(-\frac{2h_{ij}}{\sigma^2/\sigma_n^2}\right)\eta_{ij}, \tag{B9}$$

$$-\mathbb{E}\left(\frac{\partial^2 T_{ij}^2}{\partial\tau_{ij}\partial f_{D_{ij}}}\right)=0, \tag{B10}$$

$$-\mathbb{E}\left(\frac{\partial^2 T_{ij}^3}{\partial\tau_{ij}^2}\right)=\frac{8\pi^2\sigma^4}{\sigma_n^2\left(\sigma^2+\sigma_n^2\right)}\left(\frac{4h_{ij}}{\sigma^2/\sigma_n^2}\right)\varepsilon_i, \tag{B11}$$

$$-\mathbb{E}\left(\frac{\partial^2 T_{ij}^3}{\partial f_{D_{ij}}^2}\right)=\frac{8\pi^2\sigma^4}{\sigma_n^2\left(\sigma^2+\sigma_n^2\right)}\left(\frac{4h_{ij}}{\sigma^2/\sigma_n^2}\right)\eta_{ij}, \tag{B12}$$

$$-\mathbb{E}\left(\frac{\partial^2 T_{ij}^3}{\partial\tau_{ij}\partial f_{D_{ij}}}\right)=0. \tag{B13}$$

Therefore, using (13), $\mathbf{J}(\mathbf{\Psi})$ can be correspondingly expressed as follows:

$$\begin{aligned}\mathbf{J}(\mathbf{\Psi}) &= -\mathbb{E}_{\mathbf{y}(t)|\mathbf{c}}\left\{\nabla_{\mathbf{\Psi}}L(\mathbf{y}(t)|\mathbf{c})[\nabla_{\mathbf{\Psi}}L(\mathbf{y}(t)|\mathbf{c})]^{\dagger}\right\}\\ &= -\mathbb{E}_{\mathbf{y}(t)|\mathbf{c}}\left\{\nabla_{\mathbf{\Psi}}[\nabla_{\mathbf{\Psi}}L(\mathbf{y}(t)|\mathbf{c})]^{\dagger}\right\}\\ &= \sum_{i=1}^{N_t}\sum_{j=1}^{N_r}\frac{8\pi^2\sigma^4}{\sigma_n^2\left(\sigma^2+\sigma_n^2\right)}\left[1+2h_{ij}+\frac{2h_{ij}}{\left(\sigma^2/\sigma_n^2\right)}\right]\times\begin{bmatrix}\varepsilon_i & 0\\ 0 & \eta_{ij}\end{bmatrix}.\end{aligned} \tag{B14}$$

Appendix C: The Elements of MFIM $J_{ij}(\Theta)$

The elements of the symmetric MFIM $\mathbf{J}_{ij}(\mathbf{\Theta})$ corresponding to the ijth transmitter-receiver pair can be explicitly expressed as follows:

$$J_{ij}^{11}(\mathbf{\Theta})=\varepsilon_i\left(\frac{\partial\tau_{ij}}{\partial x}\right)^2+\eta_{ij}\left(\frac{\partial f_{D_{ij}}}{\partial x}\right)^2, \tag{C1}$$

$$\begin{aligned}J_{ij}^{12}(\mathbf{\Theta}) &= J_{ij}^{21}(\mathbf{\Theta})\\ &= \varepsilon_i\left(\frac{\partial\tau_{ij}}{\partial x}\right)\left(\frac{\partial\tau_{ij}}{\partial y}\right)+\eta_{ij}\left(\frac{\partial f_{D_{ij}}}{\partial x}\right)\left(\frac{\partial f_{D_{ij}}}{\partial y}\right),\end{aligned} \tag{C2}$$

$$J_{ij}^{13}(\mathbf{\Theta})=J_{ij}^{31}(\mathbf{\Theta})=\eta_{ij}\left(\frac{\partial f_{D_{ij}}}{\partial x}\right)\left(\frac{\partial f_{D_{ij}}}{\partial v_x}\right), \tag{C3}$$

$$J_{ij}^{14}(\mathbf{\Theta})=J_{ij}^{41}(\mathbf{\Theta})=\eta_{ij}\left(\frac{\partial f_{D_{ij}}}{\partial x}\right)\left(\frac{\partial f_{D_{ij}}}{\partial v_y}\right), \tag{C4}$$

$$J_{ij}^{22}(\boldsymbol{\Theta}) = \varepsilon_i \left(\frac{\partial \tau_{ij}}{\partial y}\right)^2 + \eta_{ij}\left(\frac{\partial f_{D_{ij}}}{\partial y}\right)^2, \tag{C5}$$

$$J_{ij}^{23}(\boldsymbol{\Theta}) = \eta_{ij}\left(\frac{\partial f_{D_{ij}}}{\partial y}\right)\left(\frac{\partial f_{D_{ij}}}{\partial v_x}\right), \tag{C6}$$

$$J_{ij}^{24}(\boldsymbol{\Theta}) = J_{ij}^{42}(\boldsymbol{\Theta}) = \eta_{ij}\left(\frac{\partial f_{D_{ij}}}{\partial y}\right)\left(\frac{\partial f_{D_{ij}}}{\partial v_y}\right), \tag{C7}$$

$$J_{ij}^{33}(\boldsymbol{\Theta}) = \eta_{ij}\left(\frac{\partial f_{D_{ij}}}{\partial v_x}\right)^2, \tag{C8}$$

$$J_{ij}^{34}(\boldsymbol{\Theta}) = J_{ij}^{43}(\boldsymbol{\Theta}) = \eta_{ij}\left(\frac{\partial f_{D_{ij}}}{\partial v_x}\right)\left(\frac{\partial f_{D_{ij}}}{\partial v_y}\right), \tag{C9}$$

$$J_{ij}^{44}(\boldsymbol{\Theta}) = \eta_{ij}\left(\frac{\partial f_{D_{ij}}}{\partial v_y}\right)^2. \tag{C10}$$

Acknowledgments

The authors would like to thank the anonymous reviewers for their insightful comments and suggestions that have contributed to improve this paper. We note that there are no data sharing issues since all of the numerical information is provided in the figures produced by solving the equations in the paper, which are realized by MATLAB software. This work is supported in part by the National Natural Science Foundation of China (grant 61371170 and 61671239), in part by the Fundamental Research Funds for the Central Universities (grant NS2016038 and NP2015404), in part by the National Aerospace Science Foundation of China (grant 20152052028), in part by the Priority Academic Program Development of Jiangsu Higher Education Institutions (PADA), and in part by Key Laboratory of Radar Imaging and Microwave Photonics, Ministry of Education, Nanjing University of Aeronautics and Astronautics, Nanjing, 210016, China.

References

Alam, M., and K. Jamil (2015), Maximum likelihood (ML) based localization algorithm for multistatic passive radar using range-only measurements, in *2015 IEEE Radar Conference (RadarConf)*, pp. 180–184, IEEE, Johannesburg, South Africa.

Chen, Q. C., et al. (2015), Indoor target tracking using high Doppler resolution passive WiFi radar, in *2015 IEEE International Conference on Acoustics, Speech and Signal Processing (ICASSP)*, pp. 5565–5569, IEEE, South Brisbane, Queensland, Australia.

Chen, Y. F., et al. (2013), Adaptive distributed MIMO radar waveform optimization based on mutual information, *IEEE Trans. Aerosp. Electron. Syst.*, *49*(2), 1374–1385.

Daout, F., et al. (2012), Multistatic and multiple frequency imaging resolution analysis-application to GPS-based multistatic radar, *IEEE Trans. Aerosp. Electron. Syst.*, *48*(4), 3042–3057.

Falcone, P., et al. (2014), Two-dimensional location of moving targets within local areas using WiFi-based multistatic passive radar, *IET Radar Sonar Navig.*, *8*(2), 123–131.

Filip, A., and D. Shutin (2016), Cramér-Rao bounds for L-band digital aeronautical communication system type 1 based passive multiple-input multiple-output radar, *IET Radar Sonar Navig.*, *10*(2), 348–358.

Fisher, E., et al. (2006), Spatial diversity in radars-models and detection performance, *IEEE Trans. Signal Process.*, *54*(3), 823–836.

Godrich, H., A. M. Haimovich, and R. S. Blum (2010), Target localization accuracy gain in MIMO radar-based systems, *IEEE Trans. Inf. Theory*, *56*(6), 2783–2803.

Godrich, H., A. Petropulu, and H. V. Poor (2012a), Sensor selection in distributed multiple-radar architectures for localization: A knapsack problem formulation, *IEEE Trans. Signal Process.*, *60*(1), 247–260.

Godrich, H., A. Tajer, and H. V. Poor (2012b), Distributed target tracking in multiple widely separated radar architectures, in *Proceedings of the 7th Sensor Array and Multichannel Signal Processing Workshop*, pp. 153–156, IEEE, Hoboken, N. J.

Gogineni, S., et al. (2014a), Cramér-Rao bounds for UMTS-based passive multistatic radar, *IEEE Trans. Signal Process.*, *62*(1), 95–106.

Gogineni, S., et al. (2014b), Ambiguity function analysis for UMTS-based passive multistatic radar, *IEEE Trans. Signal Process.*, *62*(11), 2945–2957.

Griffiths, H. D., and N. R. W. Long (1986), Television-based bistatic radar, 133, 649–657

Haimovich, A. M., R. S. Blum, and L. J. Jr. Cimini (2008), MIMO radar with widely separated antennas, *IEEE Signal Process Mag.*, *25*(1), 116–129.

He, Q., and R. S. Blum (2010a), Cramér-Rao bound for MIMO radar target localization with phase errors, *IEEE Signal Process Lett.*, *17*(1), 83–86.

He, Q., R. S. Blum, and A. M. Haimovich (2010b), Noncoherent MIMO radar for location and velocity estimation: More antennas means better performance, *IEEE Trans. Signal Process.*, *58*(7), 3661–3680.

He, Q., and R. S. Blum (2012), Noncoherent versus coherent MIMO radar: Performance and simplicity analysis, *Signal Process.*, *92*(10), 2454–2463.

He, Q., and R. S. Blum (2014), The significant gains from optimally processed multiple signals of opportunity and multiple receive stations in passive radar, *IEEE Signal Process. Lett.*, *21*(2), 180–184.

He, Q., et al. (2016), Generalized Cramér-Rao bound for joint estimation of target position and velocity for active and passive radar networks, *IEEE Trans. Signal Process.*, *64*(8), 2078–2089.

Howland, P. E., D. Maksimiuk, and G. Reitsma (2005), FM radio based bistatic radar, *IET Radar Sonar Navig.*, *152*(3), 107–115.

Javed, M. N., S. Ali, and S. A. Hassan (2016), 3D MCRLB evaluation of a UMTS-based passive multistatic radar operating in a line-of-sight environment, *IEEE Trans. Signal Process.*, *64*(19), 5131–5144.

Li, J., and P. Stoica (2009), *MIMO Radar Signal Processing*, Wiley, Hoboken, N. J.

Naghsh, M. M., et al. (2013), Unified optimization framework for multi-static radar code design using information-theoretic criteria, *IEEE Trans. Signal Process.*, *61*(21), 5401–5416.

Niu, R. X., et al. (2012), Target localization and tracking in noncoherent multiple-input multiple-output radar systems, *IEEE Trans. Aerosp. Electron. Syst.*, *48*(2), 1466–1489.

Pace, P. E. (2009), *Detecting and Classifying Low Probability of Intercept Radar*, Artech House, Boston, Mass.
Patzold, M., and G. Rafiq (2014), Performance evaluation of sum-of-cisoids Rice/Rayleigh fading channel simulators with respect to the bit error probability, *Radio Sci.*, *49*(1), 997–1007, doi:10.1002/2014RS005496.
Samczynski, P., P. Krysik, and K. Kulpa (2015), Passive radars utilizing pulse radars as illuminators of opportunity, in *2015 IEEE Radar Conference (RadarConf)*, pp. 168–173, IEEE, Johannesburg, South Africa.
Shi, C. G., et al. (2015), Security information factor based low probability of identification in distributed multiple-radar system, in *2015 IEEE International Conference on Acoustics, Speech and Signal Processing (ICASSP)*, pp. 3716–3720, Brisbane, Queensland, Australia.
Shi, C. G., F. Wang, and J. J. Zhou (2016a), Cramér-Rao bound analysis for joint target location and velocity estimation in FM-based passive radar networks, *IET Sign. Process.*, *10*(7), 780–790.
Shi, C. G., et al. (2016b), Transmitter subset selection in FM-based passive radar networks for joint target parameter estimation, *IEEE Sens. J.*, *16*(15), 6043–6052.
Shi, C. G., J. J. Zhou, and F. Wang (2016c), LPI based resource management for target tracking in distributed radar network, in *2016 IEEE Radar Conference (RadarConf)*, pp. 1–5, IEEE, Philadelphia, Pa.
Stinco, P., et al. (2012), Ambiguity function and Cramér-Rao bounds for universal mobile telecommunications system-based passive coherent location systems, *IET Radar Sonar Navig.*, *6*(7), 668–678.
Song, X. F., P. Willett, and S. L. Zhou (2012), Optimal power allocation for MIMO radars with heterogeneous propagation losses, in *2012 IEEE International Conference on Acoustics, Speech and Signal Processing (ICASSP)*, pp. 2465–2468, IEEE, Kyoto, Japan.
Van Trees, H. L. (2001), *Detection, Estimation, and Modulation Theory III*, Wiley, New York.
Wei, C., Q. He, and R. S. Blum (2010), Cramér-Rao bounds for joint location and velocity estimation in multi-target non-coherent MIMO radars, in *Proceedings of the 44th IEEE Annual Conference on Information Sciences and Systems (CISS)*, pp. 1–6, IEEE, Princeton, N. J.
Yi, J. X., et al. (2015), MIMO passive radar tracking under a single frequency network, *IEEE J. Sel. Top. Sign. Proces.*, *9*(8), 1661–1671.
Zhang, Z. K., S. Salous, H. L. Li, and Y. B. Tian (2015), Optimal coordination method of opportunistic array radars for multi-target-tracking-based radio frequency stealth in clutter, *Radio Sci.*, *50*(11), 1187–1196, doi:10.1002/2015RS005728.
Zhao, T., and T. Y. Huang (2016), Cramér-Rao lower bounds for the joint delay-doppler estimation of an extended target, *IEEE Trans. Signal Process.*, *64*(6), 1562–1573.